

## RESEARCH ARTICLE

10.1002/2015JA021441

## Special Section:

Variability of the Sun and Its Terrestrial Impact VarSITI

## Key Points:

- Clear 27 day solar signal in nitric oxide due to EPP production
- Epoch analysis shows the NO descent from the lower thermosphere to the mesosphere
- Suggestion as proxy for auroral electron precipitation: AE superior to Ap index

## Correspondence to:

K. Hendrickx,  
koen.hendrickx@misu.su.se

## Citation:

Hendrickx, K., L. Megner, J. Gumbel, D. E. Siskind, Y. J. Orsolini, H. Nesse Tyssøy, and M. Hervig (2015), Observation of 27 day solar cycles in the production and mesospheric descent of EPP-produced NO, *J. Geophys. Res. Space Physics*, 120, 8978–8988, doi:10.1002/2015JA021441.

Received 8 MAY 2015

Accepted 22 SEP 2015

Accepted article online 28 SEP 2015

Published online 20 OCT 2015

## Observation of 27 day solar cycles in the production and mesospheric descent of EPP-produced NO

K. Hendrickx<sup>1</sup>, L. Megner<sup>1</sup>, J. Gumbel<sup>1</sup>, D. E. Siskind<sup>2</sup>, Y. J. Orsolini<sup>3,4</sup>, H. Nesse Tyssøy<sup>4</sup>, and M. Hervig<sup>5</sup>

<sup>1</sup>Department of Meteorology, Stockholm University, Stockholm, Sweden, <sup>2</sup>Naval Research Laboratory, Washington, District of Columbia, USA, <sup>3</sup>Norwegian Institute for Air Research, Kjeller, Norway, <sup>4</sup>Birkeland Centre for Space Science, Department of Physics and Technology, University of Bergen, Bergen, Norway, <sup>5</sup>GATS Inc., Driggs, Idaho, USA

**Abstract** Nitric oxide (NO) is produced by energetic particle precipitation (EPP) in the mesosphere-lower thermosphere (MLT) region, and during the polar winter, NO can descend to stratospheric altitudes where it destroys ozone. In this paper, we study the general scenario, as opposed to a case study, of NO production in the thermosphere due to energetic particles in the auroral region. We first investigate the relationship between NO production and two geomagnetic indices. The analysis indicates that the auroral electrojet index is a more suitable proxy for EPP-produced NO than the typically used midlatitude Ap index. In order to study the production and downward transport of NO from the lower thermosphere to the mesosphere, we perform superposed epoch analyses on NO observations made by the Solar Occultation For Ice Experiment instrument on board the Aeronomy of Ice in the Mesosphere satellite. The epoch analysis clearly shows the impact of the 27 day solar cycle on NO production. The effect is observed down to an altitude range of about 50 km to 65 km, depending on the hemisphere and the occurrence of stratospheric warmings. Initially, a rapid downward transport is noted during the first 10 days after EPP onset to an altitude of about 80–85 km, which is then followed by a slower downward transport of approximately 1–1.2 km/d to lower mesospheric altitudes in the order of 30 days.

### 1. Introduction

Electrons and protons originating from both the Sun and the Earth's magnetosphere can impact the atmosphere where they interact with the present background chemical constituents ([Sinnhuber *et al.*, 2012], and references therein). The altitudes impacted by EPP depend on the type of particle and its initial energy. The frequently occurring auroral electrons (~1–10 keV) typically deposit their energy in the thermosphere down to 100 km, whereas the less frequent relativistic electrons (~1–4 MeV) can reach the lower mesosphere and stratosphere [Berger *et al.*, 1970]. The precipitating electrons will dissociate or ionize atmospheric N<sub>2</sub>, O<sub>2</sub>, and O in the mesosphere-lower thermosphere (MLT) region which on subsequent reactions will form NO<sub>x</sub> (NO+NO<sub>2</sub>) [e.g., see Barth, 1992; Porter *et al.*, 1976]. The NO concentrations have a maximum in number density in between 105 km and 110 km altitude [Siskind *et al.*, 1998] and have a lifetime of approximately 1 day or less in the mesosphere under sunlit conditions but can remain for several weeks in the polar winter [e.g., Minschwaner and Siskind, 1993; Siskind, 2000].

During polar winter and especially during Sudden Stratospheric Warming (SSW) events, the abundant NO<sub>x</sub> produced in the thermosphere by EPP can be transported downward to stratospheric altitudes [Callis and Lambeth, 1998; Randall *et al.*, 1998]. This process is referred to as the EPP indirect effect [Randall *et al.*, 2007]. NO<sub>x</sub> produced in situ in the stratosphere during intense geomagnetic storms, and solar proton events is a direct effect of EPP [e.g., Rohen *et al.*, 2005; Jackman *et al.*, 2005].

In the stratosphere, NO<sub>x</sub> can catalytically destroy ozone and therefore alter the ozone distribution and the heat budget. The transport from the lower mesosphere to stratosphere during stratospheric warmings has been investigated in both observational [e.g., Funke *et al.*, 2005; Randall *et al.*, 2009; Orsolini *et al.*, 2010; Pérot *et al.*, 2014] and model studies [e.g., Kvissel *et al.*, 2012; Tweedy *et al.*, 2013; Holt *et al.*, 2013]. Atmospheric chemistry models are able to capture this downward transport but fail to accurately represent initial NO concentrations in the lower mesosphere, indicating that insufficient NO travels downward from lower thermospheric altitudes compared to observations [e.g., Smith *et al.*, 2011; Sheese *et al.*, 2013].

In this study, we will focus on the production and transport of NO in the MLT region during and after periods of enhanced particle precipitation. We first compare the correlation of NO with two proxies of particle precipitation: the planetary  $A_p$  index and the auroral electrojet index. We then define a general scenario of EPP and investigate its impact on atmospheric NO by means of superposed epoch analyses. A description of the data sets used can be found in section 2. The results are presented in section 3 and discussed in the following subsections. In section 4, conclusions and outlook are given.

## 2. Description of Data Sets

### 2.1. AE and $A_p$ Indices

The auroral electrojet (AE) and the daily planetary  $A_p$  index are geomagnetic indices (for a detailed description, see e.g., [Menvielle et al., 2011]) and are used as proxies for EPP in atmospheric chemistry and transport models [e.g., Marsh et al., 2007]. The planetary 3-hourly  $ap$  and daily  $A_p$  indices are linearized geomagnetic indices, derived from the quasi-logarithmic  $K_p$  index. The  $A_p$  index has values ranging from 0 to 400 (corresponding to  $K_p = 0$  and  $K_p = 9$ , respectively), measured in units of 2 nT (hereinafter, we omit the units, as is often done) [Dieminger et al., 1996]. These indices represent overall geomagnetic activity over the Earth and are determined from 13 observatories stationed in the midlatitudes ( $46^\circ$  to  $63^\circ$  North and South). The magnetic perturbation here is mainly caused by the ring current, the auroral electrojet, and field-aligned current variations and shows a semiannual oscillation that peaks during equinox [Cliver et al., 2002].

The auroral electrojet has an eastward and westward component which are described, respectively, by the  $AU$  and  $AL$  geomagnetic indices. It is observed from 10 to 13 stations in the high northern latitudes in 1 min intervals. As a measure of global electrojet activity in the auroral zone, Davis and Sugiura [1966] introduced a composite index  $AE = AU - AL$  which is a direct measure of the total maximum amplitude of the auroral electrojet. The  $AE$  index has an annual cycle with minimum intensity during winter months and maximum intensity in summer, which relates to different physical processes in  $AU$  and  $AL$  due to seasonal changes in the electric field of Earth's magnetosphere [Ahn et al., 2000]. Although the physical meaning and usefulness of the  $AE$  index has been questioned [Kamide and Rostoker, 2004], it is shown by Newell and Gjerloev [2011] that the  $AE$  index correlates much better with precipitating auroral power than, e.g.,  $K_p$  or other geomagnetic indices. Based upon that result, one might expect a better correlation of NO above 100 km with the  $AE$  index rather than the planetary  $A_p$  index. Despite this, studies of NO have generally used  $A_p$  as the proxy for auroral activity [see e.g., Siskind et al., 1989; Solomon and Barth, 1999; Siskind et al., 2000; Barth and Bailey, 2004] although Sinnhuber et al. [2011] did use  $AE$ . In the current literature, there has been no systematic comparison of the relative utility of these two indices as proxies for NO production. In the following sections, we provide such a comparison.

Note that no equivalent index is available for the Southern Hemisphere; we therefore assume that EPP is symmetric between hemispheres and use  $AE$  for both. The data for the geomagnetic indices are downloaded from the World Data Center for Geomagnetism, Kyoto, and in this study we use daily averages for both  $A_p$  and  $AE$  indices.

Most particle precipitation occurs in the auroral oval region, and Solar Occultation For Ice Experiment (SOFIE) observations show that the majority of NO is produced within  $70^\circ \Lambda$  to  $80^\circ \Lambda$ , where  $\Lambda$  denotes the altitude-adjusted corrected geomagnetic latitude [Baker and Wing, 1989]. In order to make sure that the observed NO is due to direct deposition, and not meridionally transported into the region, we restrict our analysis to geomagnetic latitudes from  $65^\circ \Lambda$  to  $85^\circ \Lambda$  in this study.

### 2.2. SOFIE/AIM

The Solar Occultation For Ice Experiment (SOFIE) instrument [Gordley et al., 2009] on board of the Aeronomy of Ice in the Mesosphere (AIM) satellite began measurements on 14 May 2007 and continues until present. SOFIE performs 15 sunrise and sunset profile measurements in the Northern Hemisphere (NH) and Southern Hemisphere (SH), respectively, in 16 spectral bands, which are used to retrieve vertical profiles of, among other trace gases, nitric oxide. The NO measurements are retrieved using the  $5.32 \mu\text{m}$  absorption band, on linear volume mixing ratio (VMR) values. SOFIE retrieves NO from 30 km to 149 km altitude with an altitude resolution of approximately 2 km. The latitudinal coverage varies throughout the year from  $65^\circ$  to  $85^\circ$  latitude North and South. The NO VMR in the level 2 data products is reported on a uniform 200 m vertical grid and is, for example, used in Bailey et al. [2014] to investigate the 2013 SSW event.

Gómez-Ramírez *et al.* [2013] discusses the retrieval methods and applied corrections for the NO signal processing. Due to large thermal oscillations in the detector during the NH satellite sunrise measurements, many individual profiles are not retrievable below an altitude of 80 km in the Northern Hemisphere. In the final data product, a VMR limit of  $10^{-10}$  ppv is determined to be a lower limit where the signal-to-noise ratio is sufficient to derive concentrations of atmospheric constituents. Values below this limit were removed from the data set, prior to analysis. The reader is referred to Gómez-Ramírez *et al.* [2013] for further details.

Comparison with NO measurements from the Atmospheric Chemistry Experiment Fourier Transform Spectrometer (ACE-FTS) satellite [Bernath *et al.*, 2005] between 87 km and 105 km shows no apparent bias in SH measurements, while SOFIE showed in the NH a systematic difference in the order of  $-20\%$  to  $-30\%$  with respect to ACE-FTS below 93 km and  $-20\%$  to  $0\%$  above 93 km [see Gómez-Ramírez *et al.*, 2013]. While the data have not been formally validated above 105 km, SOFIE NO profiles were compared to NO from the Halogen Occultation Experiment (HALOE) [see Russell *et al.*, 1993]. Although they are separated by many years, SOFIE-HALOE NO differences are less than 50% for 80 km to 130 km altitude (not shown).

In this study, we use all the available SOFIE NO data (version 1.2, available on [sofie.gats-inc.com](http://sofie.gats-inc.com)) from the start of measurements until 30 April 2014.

Figure 1 shows the evolution of daily averaged NO measurements in the auroral region ( $65^\circ \Lambda$  to  $85^\circ \Lambda$ ) for the Northern and Southern Hemispheres. Effects of stratospheric warmings can be seen in the Northern Hemisphere during the polar winters of 2008/2009, 2011/2012, and 2012/2013, bringing air enriched with NO down to the middle atmosphere. The Southern Hemisphere had no stratospheric warmings during the period studied (only one was observed in 2002) [see e.g., Liu and Roble, 2005] and shows an annual cycle where NO concentrations build up and descend during winter. Due to sunlight destruction in summer [Cieslik and Nicolet, 1973], lower concentrations of NO are observed during summer than during winter at similar altitudes. In the Northern Hemispheric data, this cycle is less pronounced below 90 km due to fewer valid measurements. Short-term variations due to EPP can be seen in NO VMR in both hemispheres around 100 km altitude. Black lines indicate selected AE events which are explained in section 3.2.1.

### 3. Results

#### 3.1. Geomagnetic Indices: Proxy for NO Production

Figure 2 shows the variation of daily VMR averages of NO between 100 km and 115 km in geomagnetic latitudes of  $65^\circ$  to  $85^\circ$  during the Northern Hemispheric summers of 2008 and 2011. Also shown are the daily AE and Ap indices. The variation of NO follows the indices closely and when increases in the geomagnetic indices occur (in association with enhanced EPP), the NO concentrations will typically be enhanced 1 day later. The maximum in correlation coefficient of lower thermospheric NO with such a geomagnetic index is found with a 1 day lag in NO, in agreement with previous studies [see e.g., Solomon and Barth, 1999; Newnham *et al.*, 2013]. We show a period of 4 months in a year with low (2008) and high (2011) geomagnetic activity to highlight the differences between the indices. AE and Ap are closely correlated in the period of low geomagnetic activity but diverge from one another when the geomagnetic activity is high. We note that the correlation with NO remains high for both winter and summer time conditions, but the change in NO production per unit change in Ap or AE will be larger during winter than during summer (not shown). This is due to the competing NO destruction by sunlight during summer.

Considering the months May-June-July-August (MJJA) and November-December-January-February (NDJF) in both hemispheres, we calculated the correlation between the daily averages of the lower thermospheric NO (in between 100 and 115 km altitude) and the geomagnetic indices. Figure 3 (top) shows the correlation coefficient of NO with Ap ( $r_{NO,Ap}$ ) and AE ( $r_{NO,AE}$ ) as a function of how well AE and Ap are correlated ( $r_{AE,Ap}$ ). The correlations of the indices with NO are calculated with a 1 day lag in the latter, and the correlation coefficient values ( $r$ ) vary in number from 0.51 to 0.86. This variation in  $r$  is independent of season, year, or hemisphere, which suggests that both the AE index and the Ap index are reasonable proxies for EPP above 100 km in both hemispheres.

In order to give an indication which geomagnetic index correlates better with NO, we plot the difference  $r_{NO,Ap} - r_{NO,AE}$  as a function of  $r_{AE,Ap}$  in Figure 3 (bottom). Out of the 26 investigated periods, only 4 give a difference  $r_{NO,Ap} - r_{NO,AE}$  that is positive, i.e., a higher correlation with the Ap index, but the difference is very small ( $< 0.018$ ). In all the other periods the correlation is higher with the AE index, which suggests that it is a

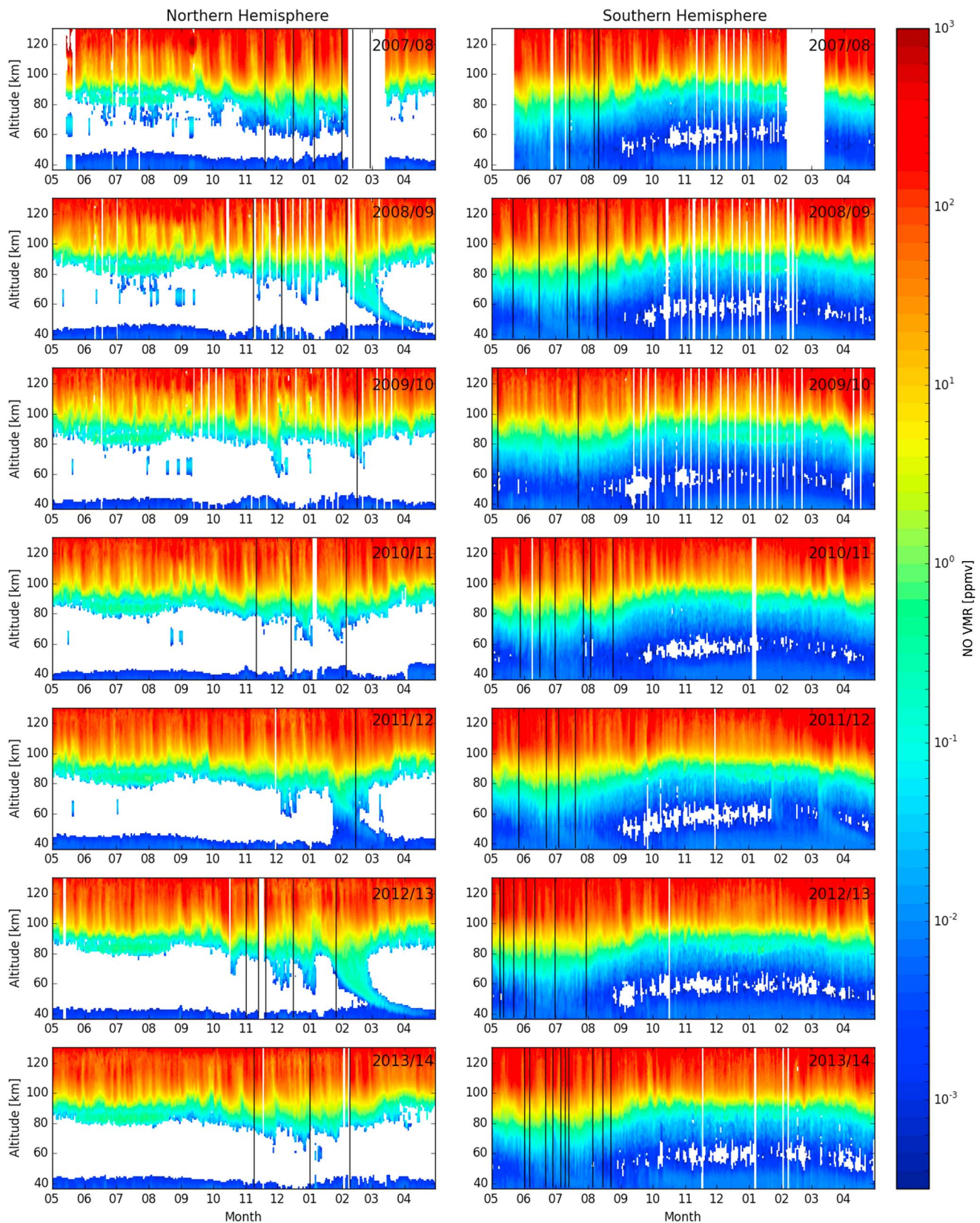


**Figure 1.** Overview of the SOFIE data set for NO volume mixing ratios, in geomagnetic latitudes from 65° to 85°, in the (left column) NH and (right column) SH for different years. White background indicates no or invalid data. Black lines indicate, respectively, 22 and 43 selected AE events in the November-December-January-February (NDJF; Figure 1, left column) and May-June-July-August (MJJA; Figure 1, right column) period, as discussed in section 3.2.1.

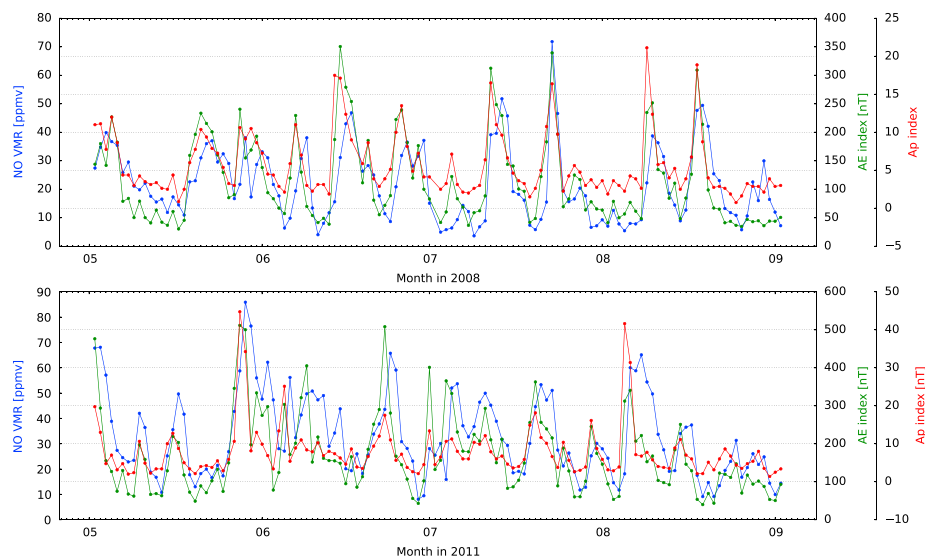


**Figure 2.** Temporal evolution of daily averages of NO VMR (blue) between 100 and 115 km, and the AE (green) and  $A_p$  (red) indices for the MJJA period in the Northern Hemispheric summer in (top) 2008 and (bottom) 2011.

more suitable proxy for auroral NO production, rather than the generally used  $A_p$  index. The differences in correlation become larger (more negative) as the mutual correlation between AE and  $A_p$  is lower. This is consistent with the result of *Newell and Gjerloev* [2011], investigating the relation of different geomagnetic indices to the auroral power. The square of the correlation coefficient  $r$  is called the coefficient of determination ( $r^2$ ) and indicates how well the data fit a linear relationship [*Draper and Smith*, 1998]. For the southern winter of 2011, the correlation coefficient of NO with the AE index is 0.75 (see Figure 3), meaning that 56% of the NO variation is explained by a linear relationship with the AE index. The coefficient of determination with the  $A_p$  index for that winter is only 30%, which indicates that the AE index is 26% better in explaining variations in NO than the  $A_p$  index. The majority of the other studied periods in Figure 3 shows that the AE index is on average around 10% better (coefficient of determination varies between 26% and  $-3\%$ ). It is to our knowledge the first time the relationship between NO and different geomagnetic indices has been investigated, and this result suggests that the auroral electrojet (AE) is a more useful geomagnetic index than the planetary  $A_p$  index as a proxy for EPP-produced NO.

### 3.2. Superposed Epoch Analysis

A statistical tool to highlight a possible response of one quantity (NO) after or before a signal in another quantity (AE) is Superposed Epoch Analysis (SEA) [e.g., *Chree*, 1913; *Robert et al.*, 2010]. In a SEA, one selects certain events according to one or more criteria and investigates the response before and after, in a chosen time window or epoch. All these events are averaged together to get the general response around an event. In order to calculate the significance levels, a Monte Carlo process is applied: over the whole data set random events and their epochs are chosen and the 68th and 95th percentiles (or  $1\sigma$  and  $2\sigma$  levels correspondingly) are calculated [*Laken and Čalogović*, 2013]. A statistically significant signal is assumed when a response value and its error bar lie above the  $1\sigma$  level. In this study, 5000 Monte Carlo iterations were performed.

NO is long lived during winter at high latitudes due to darkness but is rapidly destroyed by sunlight in the summer months. Since we are interested in the production of NO by particle precipitation, we need to remove the constant buildup that occurs especially during the winter to focus on the short-term response. The variation ( $\Delta\text{NO}$ ,  $\Delta\text{AE}$ ) is thus calculated by subtracting a smooth filter of 27 days (i.e., a box-car running mean) from the observations, a methodology similar to that of *Friederich et al.* [2014]. In order to check if this filter introduces artificial signals, a second high pass filter of 45 days was tested: the results remained unchanged. The criterion for selecting potentially enhanced EPP events is that the variation in the AE index is larger than 100 nT. The date on which this criterion is met, we mark as an AE event. The epoch around the event is  $> \pm 30$  days wide. Earth affecting solar proton events (SPE, downloaded from <http://umbra.nascom.nasa.gov/SEP/>) were removed from the analysis from the day of onset until 3 days after its maximum. However, we found that removing SPEs had no significant impact on the conclusions of the paper.

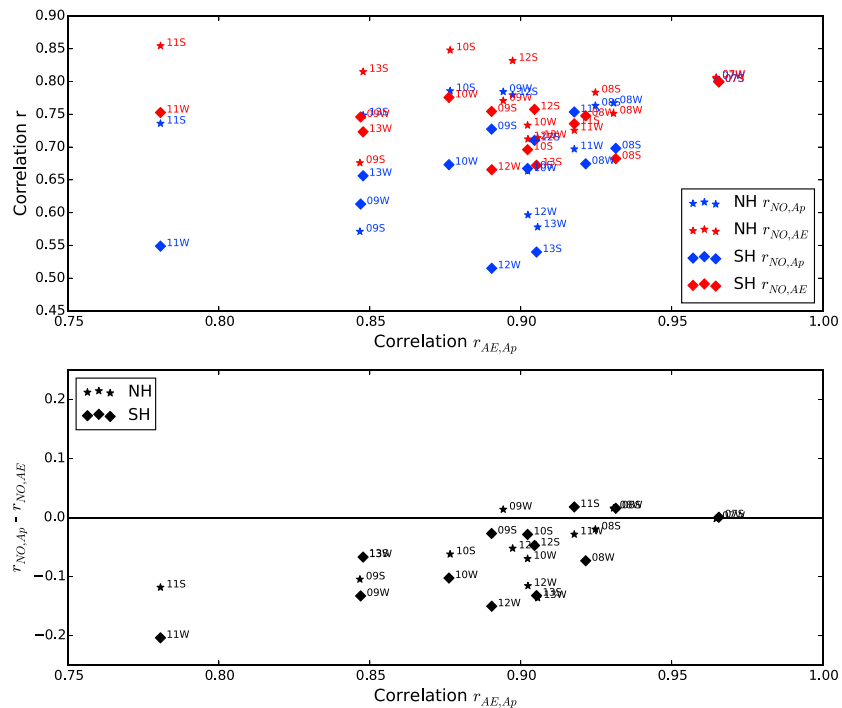


**Figure 3.** (top) Correlations of NO, lagged by 1 day, with AE (red) and Ap (blue) in both hemispheres, as function of the mutual correlation between AE and Ap ( $r_{AE,Ap}$ ). Labels show year and period: winter (W) or summer (S). (bottom) Difference of correlation between NO,Ap and NO,AE ( $r_{NO,Ap} - r_{NO,AE}$ ) as function of  $r_{AE,Ap}$ .

### 3.2.1. Effect of 27 Day Solar Cycle

Figure 4 shows results of a SEA performed on the daily variation of AE and NO. The entire data set contains 104 selected events with  $\Delta AE \geq 100$  nT. A smoothing is applied by calculating triangular averages over 3 days, with the central day having twice the weight of the other days. The NO concentrations are the average of mixing ratios between 100 km and 115 km altitude in the auroral region of the Northern (Figure 4, middle) and Southern (Figure 4, bottom) Hemispheres. The AE index shows the maximum peak at day 0 as this is the selection criteria. The AE response remains high on day 1 and returns to normal levels on day 3. Twenty seven days before and after the onset, significant increases are also seen. This 27 day cycle is due to long persisting coronal holes and the associated high-speed solar wind streams, which will then recur in line with the solar rotation [e.g., Zirker, 1977; Gopalswamy, 2008]. The response in nitric oxide shows a similar 27 day cycle and is lagged by 1 to 2 days. Days 1 and 2 have the highest NO enhancement, while the variations 27 days earlier and later are smaller by a factor of 2 or 3. The fact that the signal in NO is clearly present in both hemispheres again confirms that the AE index can be used as a proxy for EPP in the Southern Hemisphere as well.

In order to study the effects of EPP on NO in winter and summer, respectively, we analyzed the subset of the 104 selected AE events that happened in the NDJF period (and thus affected NH winter and SH summer) and the MJJA period (thus affecting SH winter and NH summer). Figure 5 (left column) shows the epoch analysis for the period NDJF which resulted in 22 selected events. Figure 5 (right column) shows 43 events in the MJJA period. The majority of these events (indicated with a black line in Figure 1) occur during the maximum and declining phase of the 11 year solar cycle, which is when the geomagnetic disturbances generally are the largest. Corotating high-speed solar wind streams make a large contribution to geomagnetic activity: they account for 70% of the geomagnetic activity during the declining phase of the solar cycle, while they account for 30% of the geomagnetic activity during solar maximum [Richardson et al., 2000], implying that the strength of the 27 day signal will vary throughout the 11 year solar cycle. In the NDJF period, 86% of the selected AE events were due to Earth facing coronal holes ([http://www.solen.info/solar/coronal\\_holes](http://www.solen.info/solar/coronal_holes)), of which 77% were reoccurring (i.e., lifetimes greater than one solar rotation), thus resulting in a clear 27 day signal. The SEA on AE variations for the 43 selected events in the MJJA period indicates a similar 27 day pattern, with  $\Delta AE \approx 145$  nT on day zero. Coronal holes account for 87% of the 43 events, of which 69% are corotating high-speed solar wind streams.

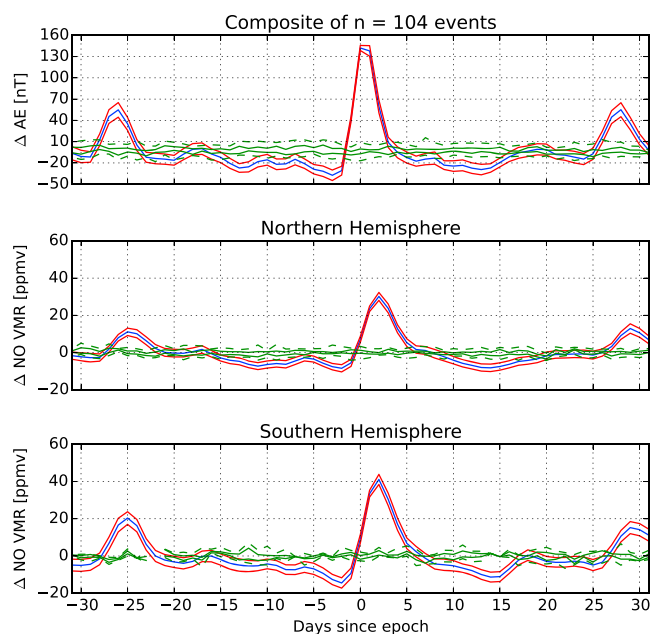


**Figure 4.** Superposed epoch analysis on the daily variation in (top) AE and vertical average of NO VMR in the lower thermosphere (in between 100 and 115 km) in the auroral region of the (middle) NH and (bottom) SH. One hundred four events were selected where  $\Delta AE \geq 100$  nT. The mean variation (blue lines) are plotted with standard errors of the mean (red lines). Solid and dashed green lines are the  $1\sigma$  and  $2\sigma$  level, respectively.

### 3.2.2. NO Response and Transport

To study the response of NO as a function of altitude, we have performed SEAs at altitudes from 35 km to 130 km in bins of 3 km and shifts of 1 km, where we selected positive NO enhancements. Figure 5 (middle row) show the impact of NO on the Northern Hemisphere, and Figure 5 (bottom row) shows the equivalent for the Southern Hemisphere. Positive NO enhancements are shown on a logarithmic color scale where the  $1\sigma$  significance levels are indicated with white contours and where the grey background represents no or negative changes in NO.

To start, we focus in Figure 5 (left column) the 22 events in the NDJF period, which correspond to NH winter and SH summer. In the northern winter, a clear 27 day cycle can be seen in the lower thermosphere that, when reaching altitudes in the mesosphere and stratosphere, shifts in time with respect to the onset of the period of enhanced AE, indicating a downward propagation of NO. Note that the logarithmic scale makes the NO mixing ratios associated with the 27 day lagged response appear of similar magnitude as the response on day zero, even though the magnitudes are a factor 2 to 3 smaller.

The strongest NO response is seen on days 1 and 2 after the AE increase starts, and direct production occurs down to altitudes of 104 km in the NH and 96 km in the SH. The general signal of elevated AE lasts for 3 days, and the significant NO production stops at day 5 at 130 km altitude, indicating that the direct production of NO by precipitating particles stops. In winter time, the lower altitude of the layer where NO variations are significant decreases from 104 km on day 0 to 84 km on day 5. While this appears to be mainly due to downward transport, there might be a contribution from direct production by more energetic particles arriving later during geomagnetic disturbances. These higher energetic electrons penetrate deeper in the atmosphere and lag the onset of the disturbance with 1 to 2 days, but their fluxes are much lower (a factor 10 to 1000 less) than the auroral electron fluxes [Meredith *et al.*, 2011]. As time progresses, the significant levels of increased NO vary between similar altitudes of 82–84 km in the span of 8 to 10 days after the initial enhancement. The descent, however, continues down to stratopause altitudes, indicating a downward transport of approximately 1 km/d, albeit not at significant levels. A similar descent rate of 1.16 km/d was found by Smith *et al.* [2011] in Whole Atmosphere Community Climate Model simulations. The loss of significance is due to less available NO data in the Northern Hemisphere, as can be seen from the NO data set in Figure 1. The 27 days before and after show a similar picture but with less NO enhancements, consistent with a weaker AE signal.

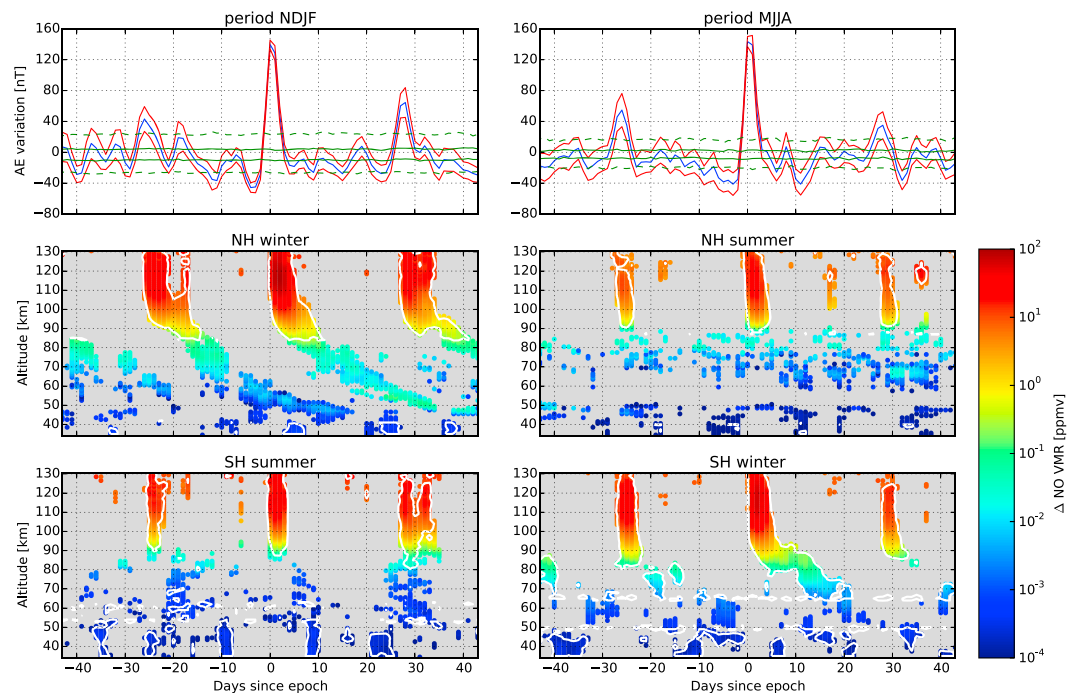


**Figure 5.** SEA performed on 22 events in the (left column) NDJF period and 43 events in the (right column) MJJA period. (top row) Variation of AE index, (middle row) NH NO enhancements, and (bottom row) SH NO enhancements. White contour lines represent  $1\sigma$  levels, and the grey background represents NO variations that are negative or consistent with zero.

The Southern Hemispheric summer shows a similar 27 day cycle with most intense NO production during the first days after the enhanced EPP period. Due to the presence of sunlight, NO will be broken down: as the input of precipitating particles subsides, NO destruction eventually dominates over direct production.

Moving to Figure 5 (right column), the 43 events in the MJJA period which correspond to NH summer and SH winter. Note that this period contains different geomagnetic disturbances than in the NDJF period, so no direct comparison can be made. In the northern summer, there are enhancements in NO above 90 km at a 27 day interval, similar to the SH summer. The direct NO production in the Southern Hemispheric winter reaches down to 92 km altitude on day 1 and 82 km on day 4 when the AE signal subsides. The following weeks NO descends to lower altitudes of 65 km on day 20 and 45 km on day 34. This suggests an approximate descend rate of 1.2 km/d in the polar vortex. A similar downward transport of NO is absent for the 27 days before and after the central day, which, as we will see, is partly explained by the lack of SSW in the SH, but may also result from the fewer reoccurring coronal holes during the MJJA period.

### 3.2.3. Influence of Stratospheric Warmings in the NH

As can be inferred from the NO data shown in Figure 1, the Northern Hemisphere is subject to sudden stratospheric warming events, which results in enhanced descent of NO-rich air [Randall et al., 2005; Kvissel et al., 2012; Bailey et al., 2014]. No SSW occurred in the Southern Hemisphere during the studied period. In the NDJF period, there are three selected AE events that occur during a stratospheric warming with prominent downward transport of NO: they occur on the dates 4 February 2009, 14 February 2012, and 26 January 2013. In order to investigate the impact of SSWs, we have excluded those events and performed a similar SEA on NO. Also, the event on 16 December 2012 was excluded since the epoch around this date includes the SSW in 2013.

Figure 6 (top) shows the NO response of 22 events with the SSW events included, while Figure 6 (bottom) shows the NO response when the SSWs are excluded (18 events). Excluding the four dates from the epoch analysis does not alter the AE variation significantly, so similar particle precipitation is expected. The production of NO above 100 km shows indeed little variation, and the downward transport remains significant to altitudes of 84 km in both cases. A weaker descent, with lower NO mixing ratios, is seen from around 70 km and downward when the SSW events are not included. Also, the descent of NO mixing ratios 27 days prior to

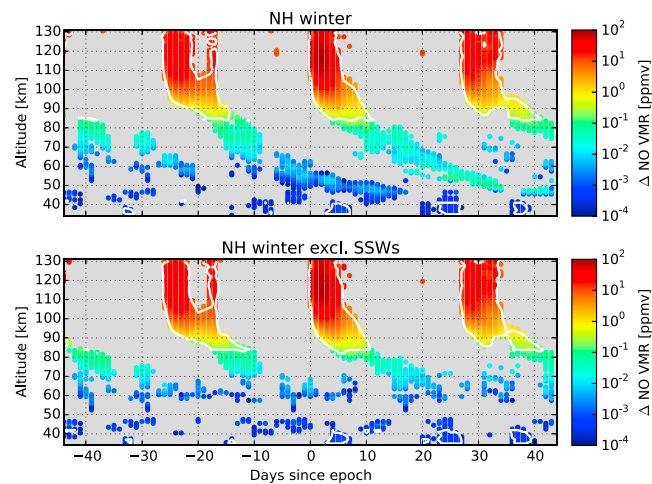


**Figure 6.** SEA performed in the NDJF period on (top) 22 and (bottom) 18 selected AE events. Figure 6 (bottom) excludes four events during the SSWs of 2008/2009, 2011/2012, and 2012/2013.

the period of enhanced EPP is weaker when the SSWs are excluded and does not seem to reach altitudes lower than 70 km in this analysis. Multiple data gaps, however, between altitudes of 50 km and 70 km in the Northern Hemisphere, affect the analysis of the downward transport in this region and make it difficult to judge how far the descent continues. Nevertheless, one can conclude that SSWs are an important phenomenon in the NH for bringing EPP-produced NO down into the lower mesosphere and upper stratosphere. In absence of SSW events, the produced NO reaches altitudes of about 70 km. In the SH, SSW events are rare: here however, the stability of the polar vortex permits NO to remain confined in the polar night where it can thus descend deeply into the stratosphere [Siskind *et al.*, 2000]. SOFIE observes the descending NO down to approximately 65 km.

#### 4. Conclusions and Outlook

In this study, epoch analyses have been used to study the general descent of EPP-produced NO, by combining 22 (43) selected AE events of enhanced particle precipitation in the Northern (Southern) Hemispheric winter. The analysis reveals that the indirect effect of EPP has a 27 day occurrence and contributes to the NO concentrations in the mesosphere. It enables us to clearly observe the effect of the 27 day solar cycle all the way down to about 50 km during the NH polar winter and approximately 65 km during the SH polar winter. Direct production of NO by EPP occurs down to an altitude of 95–105 km. In summer, the EPP-produced NO is quickly broken down after the period of enhanced particle precipitation subsides. In winter, a downward transport is seen to mesospheric altitudes and below. The initial downward motion from the lower thermosphere to the upper mesosphere is likely due to a combination of molecular and eddy diffusion processes and happens on the order of days. A further propagation to the lower mesosphere and stratopause seems to slow down to about 1–1.2 km/d.

Sudden stratospheric warmings in the Northern Hemisphere amplify this descent and are important to transport the NO anomaly down to the lower mesosphere and stratopause region. If the SSW events are excluded from the data, the downward transport reaches lower altitudes during the SH winter than during NH winters, which is to be expected given the more stable polar vortex in the Southern Hemisphere. The inferred descent rate is roughly in agreement with what is expected of the polar winter vortex descent rates from model simulations. We plan to use these results to test how well general circulation models represent the downward transport from the MLT region to the lower mesosphere and upper stratosphere. By selecting the same AE events in model simulations, one can determine, in a similar approach to the SEA used in this study, how much NO is brought downward in the atmosphere. The results can then be compared to the enhanced NO values measured by the SOFIE instrument and provide a way of validating model transport to the real atmospheric transport in a statistical sense.

Most particle precipitation occurs in the auroral region, but general circulation models typically use the mid-latitude geomagnetic indices ( $K_p$ ,  $A_p$ ) as proxies for EPP and NO production. Although these indices correlate well with the production of auroral NO, our analysis indicates that the geomagnetic auroral electrojet (AE)

index is a more suitable proxy. Nitric oxide production in the MLT region increases after periods of enhanced EPP, and the best correlation with the *AE* and *Ap* indices is found if NO is lagged by 1 day. However, the correlation coefficient values with *AE* are higher than those with the *Ap* index, independent of season or hemisphere, and the *AE* index is on average 10% better, with in individual cases up to 26% better, in explaining NO variations than the *Ap* index.

This is, to our knowledge, the first time the relationship between NO and different geomagnetic indices has been compared, and the result suggests that the auroral electrojet is a more useful geomagnetic index than the planetary *Ap* index as a proxy for particle precipitation above 100 km. We thus encourage the use of the *AE* index rather than the *Ap* index for future studies and model simulations of EPP-produced NO.

#### Acknowledgments

The authors acknowledge the World Data Center for Geomagnetism, Kyoto, for providing *AE* and *Ap* data (<http://wdc.kugi.kyoto-u.ac.jp/wdc/Sec3.html>). They also acknowledge the NOAA Space Environment Services Center for providing data on Earth affecting solar proton events (<http://umbra.nascom.nasa.gov/SEP/>). L.M. was supported by the Swedish Research Council under contract 621-2012-1648. D.E.S. and M.H. were supported by the NASA/AIM mission which is funded by NASA's Small Explorers Program under contract NAS5-03132. Y.O.R. and H.N.T. were supported by the Research Council of Norway/CoE under contract 223252/F50. K.H. and L.M. thank V.L. Harvey, S.M. Bailey, and two anonymous reviewers for helpful comments and fruitful discussions.

Michael Liemohn thanks two reviewers for their assistance in evaluating this paper.

#### References

- Ahn, B.-H., H. W. Kroehl, Y. Kamide, and E. A. Kihn (2000), Universal time variations of the auroral electrojet indices, *J. Geophys. Res.*, *105*(A1), 267–275, doi:10.1029/1999JA900364.
- Bailey, S. M., B. Thuraiajah, C. E. Randall, L. Holt, D. E. Siskind, V. L. Harvey, K. Venkataramani, M. E. Hervig, P. Rong, and J. M. Russell III (2014), A multi tracer analysis of thermosphere to stratosphere descent triggered by the 2013 Stratospheric Sudden Warming, *Geophys. Res. Lett.*, *41*, 5216–5222, doi:10.1002/2014GL059860.
- Baker, K. B., and S. Wing (1989), A new magnetic coordinate system for conjugate studies at high latitudes, *J. Geophys. Res.*, *94*(A7), 9139–9143, doi:10.1029/JA094iA07p09139.
- Barth, C. A. (1992), Nitric oxide in the lower thermosphere, *Planet. Space Sci.*, *40*(2–3), 315–336, doi:10.1016/0032-0633(92)90067-X.
- Barth, C. A., and S. M. Bailey (2004), Comparison of a thermospheric photochemical model with student nitric oxide explorer (SNOE) observations of nitric oxide, *J. Geophys. Res.*, *109*, A03304, doi:10.1029/2003JA010227.
- Berger, M. J., S. M. Seltzer, and K. Maeda (1970), Energy deposition by auroral electrons in the atmosphere, *J. Atmos. Terr. Phys.*, *32*, 1015–1045.
- Bernath, P. F., et al. (2005), Atmospheric chemistry experiment (ACE): Mission overview, *Geophys. Res. Lett.*, *32*, L15S01, doi:10.1029/2005GL022386.
- Callis, L. B., and J. D. Lambeth (1998), NO<sub>y</sub> formed by precipitating electron events in 1991 and 1992: Descent into the stratosphere as observed by ISAMS, *Geophys. Res. Lett.*, *25*(11), 1875–1878, doi:10.1029/98GL01219.
- Chree, C. (1913), Some phenomena of sunspots and of terrestrial magnetism at Kew observatory, *Philos. Trans. R. Soc. London, Ser. A*, *212*, 75–116, doi:10.1098/rsta.1913.0003.
- Cieslik, S., and M. Nicolet (1973), The aeronomic dissociation of nitric oxide, *Planet. Space Sci.*, *21*(6), 925–938, doi:10.1016/0032-0633(73)90140-2.
- Cliver, E. W., Y. Kamide, and A. G. Ling (2002), The semiannual variation of geomagnetic activity: Phases and profiles for 130 years of aa data, *J. Atmos. Sol. Terr. Phys.*, *64*(1), 47–53, doi:10.1016/S1364-6826(01)00093-1.
- Davis, T. N., and M. Sugiura (1966), Auroral electrojet activity index *AE* and its universal time variations, *J. Geophys. Res.*, *71*(3), 785–801, doi:10.1029/JZ071i003p00785.
- Dieminger, W., G. K. Hartmann, and R. Leitinger (1996), Geomagnetic activity indices, in *The Upper Atmosphere*, edited by W. Dieminger, G. Hartmann, and R. Leitinger, pp. 887–911, Springer, Berlin, doi:10.1007/978-3-642-78717-1.
- Draper, N. R., and H. Smith (1998), *Fitting a Straight Line by Least Squares*, pp. 15–46, John Wiley, doi:10.1002/9781118625590.ch1.
- Friederich, F., M. Sinnhuber, B. Funke, T. von Clarmann, and J. Orphal (2014), Local impact of solar variation on NO<sub>2</sub> in the lower mesosphere and upper stratosphere from 2007 to 2012, *Atmos. Chem. Phys.*, *14*(8), 4055–4064, doi:10.5194/acp-14-4055-2014.
- Funke, B., M. López-Puertas, S. Gil-López, T. von Clarmann, G. P. Stiller, H. Fischer, and S. Kellmann (2005), Downward transport of upper atmospheric NO<sub>x</sub> into the polar stratosphere and lower mesosphere during the Antarctic 2003 and Arctic 2002/2003 winters, *J. Geophys. Res.*, *110*, D24308, doi:10.1029/2005JD006463.
- Gómez-Ramírez, D., W. C. McNabb, J. M. Russell, M. E. Hervig, L. E. Deaver, G. Paxton, and P. F. Bernath (2013), Empirical correction of thermal responses in the solar occultation for ice experiment nitric oxide measurements and initial data validation results, *Appl. Opt.*, *52*(13), 2950–2959, doi:10.1364/ao.52.002950.
- Gopalswamy, N. (2008), Solar connections of geoeffective magnetic structures, *J. Atmos. Sol. Terr. Phys.*, *70*, 2078–2100, doi:10.1016/j.jastp.2008.06.010.
- Gordley, L. L., et al. (2009), The solar occultation for ice experiment, *J. Atmos. Sol. Terr. Phys.*, *71*(3–4), 300–315, doi:10.1016/j.jastp.2008.07.012.
- Holt, L. A., C. E. Randall, E. D. Peck, D. R. Marsh, A. K. Smith, and V. L. Harvey (2013), The influence of major sudden stratospheric warming and elevated stratospheric events on the effects of energetic particle precipitation in WACCM, *J. Geophys. Res. Atmos.*, *118*, 11,636–11,646, doi:10.1002/2013JD020294.
- Jackman, C. H., M. T. DeLand, G. J. Labow, E. L. Fleming, D. K. Weisenstein, M. K. W. Ko, M. Sinnhuber, and J. M. Russell (2005), Neutral atmospheric influences of the solar proton events in October November 2003, *J. Geophys. Res.*, *110*, A09S27, doi:10.1029/2004JA010888.
- Kamide, Y., and G. Rostoker (2004), What is the physical meaning of the *AE* index?, *Eos Trans. AGU*, *85*(19), 188–192, doi:10.1029/2004EO190010.
- Kvissel, O.-K., Y. J. Orsolini, F. Stordal, V. Limpasuvan, J. Richter, and D. R. Marsh (2012), Mesospheric intrusion and anomalous chemistry during and after a major Stratospheric Sudden Warming, *J. Atmos. Sol. Terr. Phys.*, *78–79*, 116–124, doi:10.1016/j.jastp.2011.08.015.
- Laken, B. A., and J. Čalogović (2013), Composite analysis with Monte Carlo methods: An example with cosmic rays and clouds, *J. Space Weather Space Clim.*, *3*(A29), doi:10.1051/swsc/2013051.
- Liu, H., and R. G. Roble (2005), Dynamical coupling of the stratosphere and mesosphere in the 2002 Southern Hemisphere major Stratospheric Sudden Warming, *Geophys. Res. Lett.*, *32*, L13804, doi:10.1029/2005GL022939.
- Marsh, D. R., R. R. Garcia, D. E. Kinnison, B. A. Boville, F. Sassi, S. C. Solomon, and K. Matthes (2007), Modeling the whole atmosphere response to solar cycle changes in radiative and geomagnetic forcing, *J. Geophys. Res.*, *112*, D23306, doi:10.1029/2006JD008306.
- Menvielle, M., T. Iyemori, A. Marchaudon, and M. Nosé (2011), Geomagnetic indices, in *Geomagnetic Observations and Models*, vol. 5, edited by M. Mandaia and M. Korte, pp. 183–228, IAGA Special Sopron Book Series, Springer, Netherlands, doi:10.1007/978-90-481-9858-0.
- Meredith, N. P., R. B. Horne, M. M. Lam, M. H. Denton, J. E. Borovsky, and J. C. Green (2011), Energetic electron precipitation during high-speed solar wind stream driven storms, *J. Geophys. Res.*, *116*, A05223, doi:10.1029/2010JA016293.

- Minschwaner, K., and D. E. Siskind (1993), A new calculation of nitric oxide photolysis in the stratosphere, mesosphere, and lower thermosphere, *J. Geophys. Res.*, *98*, 20,401–20,412, doi:10.1029/93JD02007.
- Newell, P. T., and J. W. Gjerloev (2011), Evaluation of SuperMAG auroral electrojet indices as indicators of substorms and auroral power, *J. Geophys. Res.*, *116*, A12211, doi:10.1029/2011JA016779.
- Newnham, D. A., P. J. Espy, M. A. Clilverd, C. J. Rodger, A. Seppälä, D. J. Maxfield, P. Hartogh, C. Straub, K. Holmén, and R. B. Horne (2013), Observations of nitric oxide in the antarctic middle atmosphere during recurrent geomagnetic storms, *J. Geophys. Res. Space Physics*, *118*, 7874–7885, doi:10.1002/2013JA019056.
- Orsolini, Y. J., J. Urban, D. P. Murtagh, S. Lossow, and V. Limpasuvan (2010), Descent from the polar mesosphere and anomalously high stratopause observed in 8 years of water vapor and temperature satellite observations by the Odin sub-millimeter radiometer, *J. Geophys. Res.*, *115*, D12305, doi:10.1029/2009JD013501.
- Pérot, K., J. Urban, and D. P. Murtagh (2014), Unusually strong nitric oxide descent in the arctic middle atmosphere in early 2013 as observed by Odin/SMR, *Atmos. Chem. Phys.*, *14*(15), 8009–8015, doi:10.5194/acp-14-8009-2014.
- Porter, H. S., C. H. Jackman, and A. E. S. Green (1976), Efficiencies for production of atomic nitrogen and oxygen by relativistic proton impact in air, *J. Chem. Phys.*, *65*(1), 154, doi:10.1063/1.432812.
- Randall, C. E., D. W. Rusch, R. M. Bevilacqua, K. W. Hoppel, and J. D. Lumpe (1998), Polar ozone and aerosol measurement (POAM) II stratospheric NO<sub>2</sub>, 1993–1996, *J. Geophys. Res.*, *103*(D21), 28,361–28,371, doi:10.1029/98JD02092.
- Randall, C. E., et al. (2005), Stratospheric effects of energetic particle precipitation in 2003–2004, *Geophys. Res. Lett.*, *32*, L05802, doi:10.1029/2004GL022003.
- Randall, C. E., V. L. Harvey, C. S. Singleton, S. M. Bailey, P. F. Bernath, M. Codrescu, H. Nakajima, and J. M. Russell (2007), Energetic particle precipitation effects on the Southern Hemisphere stratosphere in 1992–2005, *J. Geophys. Res.*, *112*, D08308, doi:10.1029/2006JD007696.
- Randall, C. E., V. L. Harvey, D. E. Siskind, J. France, P. F. Bernath, C. D. Boone, and K. A. Walker (2009), NO<sub>x</sub> descent in the Arctic middle atmosphere in early 2009, *Geophys. Res. Lett.*, *36*, L18811, doi:10.1029/2009GL039706.
- Richardson, I. G., E. W. Cliver, and H. V. Cane (2000), Sources of geomagnetic activity over the solar cycle: Relative importance of coronal mass ejections, high speed streams, and slow solar wind, *J. Geophys. Res.*, *105*(A8), 18,203–18,213, doi:10.1029/1999JA000400.
- Robert, C. E., C. von Savigny, N. Rahpoe, H. Bovensmann, J. P. Burrows, M. T. DeLand, and M. J. Schwartz (2010), First evidence of a 27 day solar signature in noctilucent cloud occurrence frequency, *J. Geophys. Res.*, *115*, D00112, doi:10.1029/2009JD012359.
- Rohen, G., et al. (2005), Ozone depletion during the solar proton events of October/November 2003 as seen by SCIAMACHY, *J. Geophys. Res.*, *110*, A09539, doi:10.1029/2004JA010984.
- Russell, J. M., L. L. Gordley, J. H. Park, S. R. Drayson, W. D. Hesketh, R. J. Cicerone, A. F. Tuck, J. E. Frederick, J. E. Harries, and P. J. Crutzen (1993), The halogen occultation experiment, *J. Geophys. Res.*, *98*(D6), 10,777–10,797, doi:10.1029/93JD00799.
- Sheese, P. E., K. Strong, R. L. Gattinger, E. J. Llewellyn, J. Urban, C. D. Boone, and A. K. Smith (2013), Odin observations of Antarctic nighttime NO densities in the mesosphere-lower thermosphere and observations of a lower NO layer, *J. Geophys. Res. Atmos.*, *118*, 7414–7425, doi:10.1002/jgrd.50563.
- Sinnhuber, M., S. Kazeminejad, and J. M. Wissing (2011), Interannual variation of NO<sub>x</sub> from the lower thermosphere to the upper stratosphere in the years 1991–2005, *J. Geophys. Res.*, *116*, A02312, doi:10.1029/2010JA015825.
- Sinnhuber, M., H. Nieder, and N. Wieters (2012), Energetic particle precipitation and the chemistry of the mesosphere/lower thermosphere, *Surv. Geophys.*, *33*(6), 1281–1334, doi:10.1007/s10712-012-9201-3.
- Siskind, D. E. (2000), *On the Coupling Between Middle and Upper Atmospheric Odd Nitrogen*, pp. 101–116, AGU, Washington, D. C., doi:10.1029/GM123p0101.
- Siskind, D. E., C. A. Barth, D. S. Evans, and R. G. Roble (1989), The response of thermospheric nitric oxide to an auroral storm: 2. Auroral latitudes, *J. Geophys. Res.*, *94*(A12), 16,899–16,911, doi:10.1029/JA094A12p16899.
- Siskind, D. E., C. A. Barth, and J. M. Russell (1998), A climatology of nitric oxide in the mesosphere and thermosphere, *Adv. Space Res.*, *21*(10), 1353–1362, doi:10.1016/S0273-1177(97)00743-6.
- Siskind, D. E., G. E. Nedoluha, C. E. Randall, M. Fromm, and J. M. Russell (2000), An assessment of Southern Hemisphere stratospheric NO<sub>x</sub> enhancements due to transport from the upper atmosphere, *Geophys. Res. Lett.*, *27*(3), 329–332, doi:10.1029/1999GL010940.
- Smith, A. K., R. R. Garcia, D. R. Marsh, and J. H. Richter (2011), WACCM simulations of the mean circulation and trace species transport in the winter mesosphere, *J. Geophys. Res.*, *116*, D20115, doi:10.1029/2011JD016083.
- Solomon, S. C., and C. A. Barth (1999), Auroral production of nitric oxide measured by the SNOE satellite, *Geophys. Res. Lett.*, *26*(9), 1259–1262, doi:10.1029/1999GL900235.
- Tweedy, O. V., et al. (2013), Nighttime secondary ozone layer during major stratospheric sudden warmings in specified dynamics WACCM, *J. Geophys. Res. Atmos.*, *118*, 8346–8358, doi:10.1002/jgrd.50651.
- Zirker, J. B. (1977), Coronal holes and high-speed wind streams, *Rev. Geophys.*, *15*(3), 257–269, doi:10.1029/RG015i003p00257.